JOURNAL OF GUIDANCE, CONTROL, AND DYNAMICS
Vol. 32, No. 3, May–June 2009

Properties of a Real-Time Guidance Method for Preventing a Collision

David J. Gates*
Commonwealth Scientific and Industrial Research Organization, Canberra, Australian Capital Territory 2601, Australia

DOI: 10.2514/1.41197

This paper studies a real-time coordination method for preventing a midair collision between two aircraft. The aircraft obey guidance laws in which the directions of the command accelerations are based on the predicted positions of the aircraft at closest approach if their velocity vectors were not to change. A general form of the magnitude of these accelerations is studied, but a simple aircraft model is used. The differential equations of motion have the form of Newtonian two-body dynamics, with some nonstandard complications. The equations are readily solved numerically, but a general mathematical description of the motion for all configurations is vital for this application. The description is quite complex, involving twisting and intertwining paths in three dimensions. It is proved that the motion always has some basic desirable features of evasion. The guidance implies a logical set of turning rules, which are more effective than the common rules of the air. If the aircraft are similar, the paths have various symmetries and congruencies and can be described fairly completely. In some cases, the paths are arcs of circles. Some exact solutions are given for planar motion. These provide control over minimum separation and accommodate limits on turn rates. There is a close connection with a cockpit display described recently, and so the results also support the effectiveness of the display.

Nomenclature

$\boldsymbol{a}_i$	=	lateral acceleration vector of aircraft i, m/s^2
f_i	=	force constant for lateral acceleration of aircraft i, m/s^2
$\boldsymbol{K}_i$	=	curvature vector of path of aircraft i, /m
$\boldsymbol{M}$	=	vector from aircraft 1 to aircraft 2 at closest approach of their extrapolated paths, m
M	=	magnitude of $\boldsymbol{M}$, m
$\boldsymbol{m}$	=	unit vector along $\boldsymbol{M}$, dimensionless
$\bar{\boldsymbol{m}}_i$	=	component vector of $\boldsymbol{m}$ normal to $\boldsymbol{V}_i$, dimensionless
$\boldsymbol{o}_R$	=	unit vector along $\boldsymbol{\Omega}_R$, dimensionless
p_i	=	gain constant for aircraft i, dimensionless
$\boldsymbol{r}_i$	=	position vector of aircraft i, m
$\boldsymbol{r}_R$	=	position vector of aircraft 2 relative to aircraft 1, m
r_R	=	distance between centers of aircraft 1 and 2, m
t	=	time, s
t_R	=	time to closest approach of the extrapolated paths of aircraft 1 and 2, s
$\boldsymbol{u}_i$	=	unit vector along $\boldsymbol{V}_i$, dimensionless
$\boldsymbol{V}_i$	=	velocity vector of aircraft i, m/s
V_i	=	speed of aircraft i, m/s
$\boldsymbol{V}_R$	=	velocity vector of aircraft 2 relative to aircraft 1, m/s
V_R	=	magnitude of $\boldsymbol{V}_R$, m/s
$\boldsymbol{w}_R$	=	unit vector along $\boldsymbol{V}_R$, dimensionless
$\boldsymbol{\Gamma}_i$	=	angular velocity vector of aircraft i, rad/s
$\kappa_i(t)$	=	curvature of path of aircraft i at time t, /m
$\tau_i(t)$	=	torsion of path of aircraft i at time t, /m
ϕ_R	=	angle between $\boldsymbol{V}_1$ and $\boldsymbol{V}_2$, radians
$\boldsymbol{\Omega}_R$	=	angular velocity vector of $\boldsymbol{r}_R$, rad/s
Ω_R	=	magnitude of $\boldsymbol{\Omega}_R$, rad/s

Received 24 September 2008; revision received 7 February 2009; accepted for publication 9 February 2009.

*Research Scientist, Optimisation in Air Transport Management Team, Mathematical and Information Sciences, GPO Box 664; david.gates@csiro.au.

I. Introduction

AS A last resort, when a collision between two aircraft is imminent, the aircraft could conceivably be steered onto safe courses by automated control. Experimental systems with this purpose [1,2] have been developed for small jet aircraft, and preliminary tests have been carried out. For small maneuverable aircraft, automated guidance might be active for a matter of seconds. For large passenger aircraft, the time scale might be of the order of a minute, as in the Traffic Alert and Collision Avoidance System (TCAS II), which provides automated advice, but not control. In such dynamic situations, in which path planning is not possible, one needs a form of real-time coordination, in which command accelerations are based on the situation at each instant of time and cause each aircraft to turn and climb or descend. Such methods can be robust or adaptive, in the sense that they remain effective even if the aircraft have previously failed to achieve their command accelerations. In such methods, each aircraft needs continuous accurate information about the positions and velocities of both aircraft, and this is becoming available through integrated inertial navigation systems (INS) and the Global Positioning System (GPS) [3].

The command accelerations in real-time coordination have traditionally been based on fictitious forces, resembling forces between atomic-scale particles in physics. Thus, the motion can be regarded as the result of forces of interaction between the vehicles. Such guidance laws have their origin in obstacle avoidance by robot vehicles, using fictitious electrostatic (Coulomb) forces [4–6]. However, these forces can produce inefficient evasion and can create local minima in the potential field that can trap a vehicle. Some variants of this method [7–9] are able to avoid local minima. The inherent limitations of the electrostatic model have led to models involving magnetic fields [10] and other vector fields [11,12] and their application to mutually avoiding vehicles. Different again are models based on fluid dynamics [13], sliding motion [14,15], and vortex fields [16,17].

Real Coulomb repulsion of electrically charged spacecraft has an application to collision prevention [18–20]. Methods based on the mathematics of optimal control theory have been used to plan energy-efficient collision-free aircraft paths on a longer time scale [21–23] and to plan collision-free formation flying of spacecraft [24,25]. These methods generate optimal paths, but do not control the vehicles. They can be supplemented by real-time guidance to cause the vehicles to follow such paths [26]. Various methods are reviewed

and compared in [27,28]. Another development [29] is the augmentation of aircraft control, so that pilots can directly command specific turns via built-in control logic. This is not quite automated guidance, but it is less intrusive.

Gazit and Powell [3] (Sec. 5, Method 2) and Zeghal [15,30] independently studied a form of real-time coordination based on the following principle. If two aircraft are on convergent paths and were to continue with their current velocity vectors, they would reach a configuration of least separation, called the expected (or extrapolated) closest point of approach (ECPA). The expected miss vector $\boldsymbol{M}$ is the 3-D vector, directed from aircraft 1 to aircraft 2 at the ECPA. The command accelerations are formulated in terms of $\boldsymbol{M}$, with the purpose of increasing the expected miss distance (EMD) $M = |\boldsymbol{M}|$. Zeghal [30] carried out a large number of computer simulations of this EMD guidance with many vehicles. He demonstrated that it performs well according to measures of effectiveness and efficiency and greatly outperforms electrostatic repulsion. The essential reason is that EMD guidance allows crossing paths and milder turns. It is much less likely to produce commands that exceed the capability of the vehicle.

The emphasis in [30] is on longer-term path coordination of many vehicles, but the principle of EMD guidance seems well suited to the automated evasion of two aircraft at close quarters, on or near a collision course. For such an application, the outcomes need to be thoroughly understood for all possible scenarios. However, EMD guidance has not been previously studied by mathematical, as opposed to numerical, methods, and no analytic solutions have hitherto been published, and so very little is known about it in general. Here, a general form of the force law is studied, and the resulting motion is described in qualitative and geometric terms. The main results are presented as formal theorems, because, in such a critical application, one needs to prove various properties of the motion beyond any doubt. These properties cannot be guaranteed by any number of simulations.

It will also be shown that EMD guidance is completely consistent with a new cockpit display [31], in which values of EMD are projected. It follows that many of the results about EMD guidance also support the effectiveness of the display. General results of this sort about a cockpit display seem to be quite novel and very desirable. Displays are usually tested in simulators using selected scenarios. Inevitably, the scenarios tested are only a small fraction of the possibilities, and so general conclusions about the safety of a display are difficult to draw.

This paper is organized as follows. Section II defines the guidance law and illustrates trajectories. Section III gives some mathematical preliminaries. Section IV draws analogies with two-body Newtonian dynamics. Section V describes the variation of separation and EMD with time. Section VI classifies turning directions caused by EMD guidance, in terms of relative speed and relative heading. Sections VII and VIII study the motion of aircraft that are similar and have equal speeds. Section IX shows that EMD guidance is effective when only one aircraft is guided. Section X gives a geometric formulation of EMD guidance. Section XI gives some exact solutions for planar motion, which provide controls on minimum separation and accommodate limits on turning capability. Section XII considers the cockpit display and can be read after Sec. III. Section XIII draws conclusions and mentions possible extensions of the work. This paper adopts the convention from kinematics in which the velocity is a vector and the speed is the magnitude of the vector.

II. EMD Guidance

In this section, EMD guidance is defined and illustrated. As mentioned, guidance is formulated in terms of the miss vector $\boldsymbol{M}$, illustrated in Fig. 1. If the aircraft are too close and M is too small, the aircraft should be steered to increase M. Aircraft 2 should therefore steer toward $\boldsymbol{M}$ and aircraft 1 should steer toward $-\boldsymbol{M}$, as indicated in Fig. 1.

The greatest effect is obtained if aircraft 1 turns in the instantaneous plane of $\boldsymbol{V}_1$ and $-\boldsymbol{M}$, and so it should turn about an axis in the direction of $\boldsymbol{V}_1 \times (-\boldsymbol{M})$. One seeks to maintain aircraft speed, and so the only component of acceleration of the aircraft must be perpendicular to its velocity. In practice, speeds do not change significantly in the short time scales relevant here, and so the constant speed model is often realistic. Let $\boldsymbol{u}_i$ and $\boldsymbol{m}$ denote the unit vectors along $\boldsymbol{V}_i$ and $\boldsymbol{M}$, respectively. Then aircraft 1 is given a lateral acceleration $\boldsymbol{a}_1$ (Fig. 1) in the direction of $-\bar{\boldsymbol{m}}_1$, where

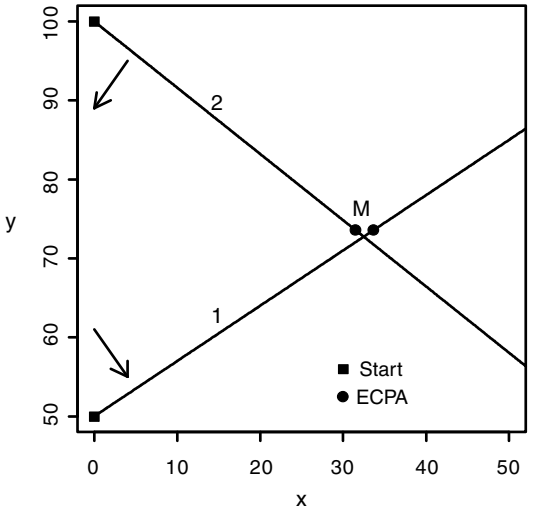

Fig. 1 The miss vector M goes from A/C 1 to A/C 2 at the ECPA. The arrows indicate the directions of the initial accelerations a_i. The distance scale depends on the situation here and henceforth.

$$\bar{\boldsymbol{m}}_i = \boldsymbol{u}_i \times \boldsymbol{m} \times \boldsymbol{u}_i \tag{1}$$

is the component of $\boldsymbol{m}$ normal to $\boldsymbol{u}_i$, and $i = 1, 2$. Brackets are omitted from Eq. (1) and henceforth without ambiguity, because $\boldsymbol{u} \times (\boldsymbol{m} \times \boldsymbol{u}) = (\boldsymbol{u} \times \boldsymbol{m}) \times \boldsymbol{u}$. Thus,

$$\boldsymbol{a}_1 = -f_1 \bar{\boldsymbol{m}}_1 \tag{2}$$

where the force coefficients $f_i > 0$ depend on the current situation and the type of aircraft. For example, a larger, less agile aircraft might be assigned a smaller f_i. Similarly, aircraft 2 is given a lateral acceleration:

$$\boldsymbol{a}_2 = f_2 \bar{\boldsymbol{m}}_2 \tag{3}$$

An aircraft's location is identified with a suitable center point of the aircraft, such as the center of the minimum enclosing sphere. Then one can say that aircraft i has position vector $\boldsymbol{r}_i(t)$ and velocity vector $\boldsymbol{V}_i(t)$ at time t. Each aircraft is modeled with only 3 degrees of freedom. Then the motion of each aircraft is determined by the differential equations:

$$\dot{\boldsymbol{r}}_i = \boldsymbol{V}_i, \qquad \dot{\boldsymbol{V}}_i = \boldsymbol{a}_i \tag{4}$$

where the overdot indicates a time derivative. This is a general form of EMD guidance. The two aircraft follow curved paths induced by the lateral accelerations. If $M = 0$, then $\boldsymbol{m}$ is not defined. If this happens initially, then the initiation of guidance must be carefully managed, as described at the end of Sec. VI.

As a simple illustration, consider the case in which aircraft 2 is replaced by a stationary obstacle. Then Eq. (2) reduces to

$$\boldsymbol{a}_1 = -f_1 \boldsymbol{m} \tag{5}$$

and so the acceleration is directed exactly along the expected miss vector away from obstacle 2. Because $\boldsymbol{M}$ lies in the plane of $\boldsymbol{r}_R$ and $\boldsymbol{u}_1$, the motion of the aircraft remains in the plane defined by the initial values of $\boldsymbol{r}_R$ and $\boldsymbol{u}_1$. If f_1 is constant, the path is an arc of a circle, as Eq. (42) shows, which seems not to have been noted before. This is a common and convenient aircraft maneuver.

Figure 2 illustrates the planar motion of two aircraft with force coefficients

$$f_i = \frac{p_i V_i^2}{r_R} \tag{6}$$

where p_i are the dimensionless gain constants, $V_i = |\boldsymbol{V}_i|$ are the speeds, and $r_R = |\boldsymbol{r}_2 - \boldsymbol{r}_1|$ is the current separation. The values $p_1 = p_2 = 0.5$ are used, and the initial conditions are as in Fig. 1, in which the headings make angles of 35 and -40 deg with the x axis. The distance scale is in arbitrary units, which could be chosen according to the type of aircraft. The aircraft have equal speeds, but the magnitudes of the speeds do not affect the paths, as shown in Sec. X, and so they are not specified. Aircraft 2 turns behind aircraft 1, illustrating the efficiency of the maneuvers. Figure 3 shows how r_R and M vary with distance along a path, which is proportional to time. This paper is mainly devoted to proving general properties of the motion illustrated here, and of 3-D motion, which is illustrated later.

The force coefficients in Eq. (6) imply harder turning at smaller separations, in which evasion is more urgent. This also provides an adaptive response to guidance deficiencies. For example, if the achieved accelerations fall short of the command accelerations, then r_R will become smaller than anticipated. Hence, subsequent command accelerations will be larger than anticipated and tend to compensate for the shortfall.

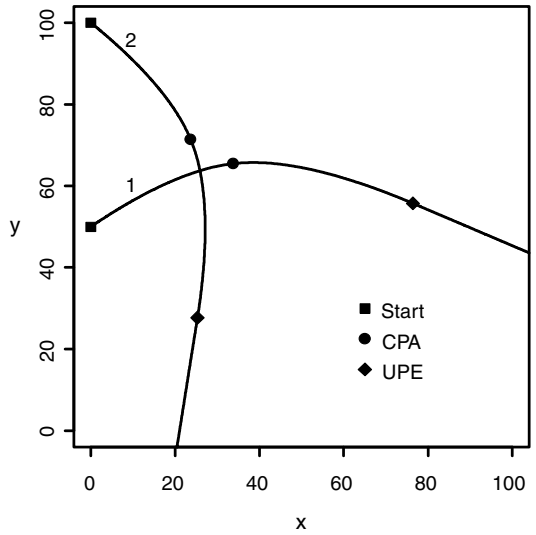

Fig. 2 Paths of the aircraft with the initial configuration in Fig. 1.

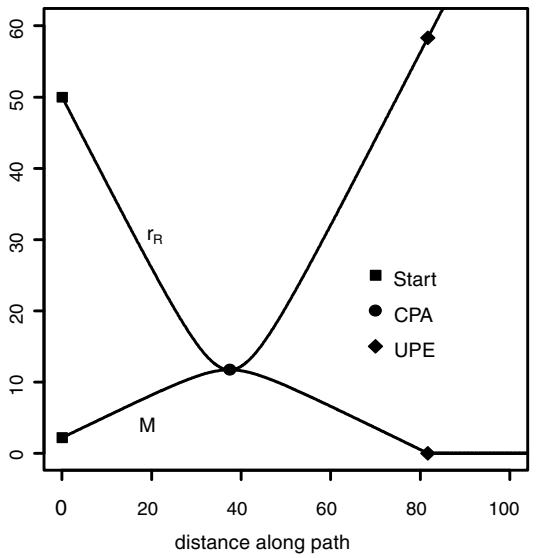

Fig. 3 The change in separation r_R and projected miss distance M with the distance traveled by either aircraft along its path.

The aircraft reach the real closest point of approach (CPA) (Fig. 2) distinct from the time-varying ECPA. Beyond the CPA, the aircraft are receding and the conflict could be regarded as resolved. One might therefore choose to terminate evasion at the CPA or shortly thereafter. This would lead to fairly obvious modifications. One could also then activate some form of path-following guidance [26] to return the aircraft to their original paths. However, in critical situations on short time scales, this is a secondary consideration and is not mentioned further. In fact, the evasion reaches a natural termination point, as shown in Theorem 3.

A larger spherical protection zone can be centered on $\boldsymbol{r}_i$. The breaching of a protection zone occurs when r_R falls below a critical value. This has relevance on longer time scales, on which a safe separation is feasible.

There are practical factors when implementing such laws in real aircraft. Techniques of control and feedback are well-developed for such a purpose [32]. The effect of wind can be significant. For large aircraft, in particular, one should distinguish between horizontal and vertical maneuvers, in which factors to consider are aircraft capabilities, surrounding traffic, and passenger safety. Note that TCAS advises only vertical maneuvers, partly because of inadequate horizontal data, but this might change as INS–GPS systems are incorporated. In critical situations, limits on aircraft capability might be the dominant factor. Turning limits are studied in Sec. XI.

III. Kinematic Preliminaries

In this section, some general kinematic results are obtained. These do not describe EMD guidance as such, but are necessary for subsequent analysis of the guidance law. Simple geometry shows that [3]

$$\boldsymbol{M} = \begin{cases} \boldsymbol{w}_R \times \boldsymbol{r}_R \times \boldsymbol{w}_R & \text{if } \boldsymbol{V}_1 \neq \boldsymbol{V}_2 \\ \boldsymbol{r}_R & \text{otherwise} \end{cases} \tag{7}$$

where $\boldsymbol{r}_R = \boldsymbol{r}_2 - \boldsymbol{r}_1$ is the current relative position vector from aircraft 1 to aircraft 2, and $\boldsymbol{w}_R$ is the unit vector along the velocity of aircraft 2 relative to aircraft 1:

$$\boldsymbol{V}_R = \dot{\boldsymbol{r}}_R = \boldsymbol{V}_2 - \boldsymbol{V}_1 \tag{8}$$

Thus, $\boldsymbol{M}$ is the component of $\boldsymbol{r}_R$ normal to $\boldsymbol{V}_R$. Although the ECPA refers to a (hypothetical) future event, $\boldsymbol{M}$ depends only on the state of the aircraft at the current time t. Some other expressions for $\boldsymbol{M}$ are useful. First, if $\boldsymbol{V}_1 \neq \boldsymbol{V}_2$, one can write

$$\boldsymbol{M} = \boldsymbol{r}_R - (\boldsymbol{r}_R \cdot \boldsymbol{w}_R)\boldsymbol{w}_R = \boldsymbol{r}_R + t_R \boldsymbol{V}_R \tag{9}$$

where

$$t_R(t) = -\frac{\boldsymbol{r}_R \cdot \boldsymbol{w}_R}{V_R} \tag{10}$$

is the time for the extrapolated straight motions to reach ECPA [30]. Here, V_R is the magnitude of $\boldsymbol{V}_R$. If one defines $t_R = 0$ when $\boldsymbol{V}_1 = \boldsymbol{V}_2$, then Eq. (9) extends to this case. As $\boldsymbol{M} \perp \boldsymbol{V}_R$, one has

$$M^2 = r_R^2 - V_R^2 t_R^2 \tag{11}$$

and so $M \leq r_R$. The angular velocity vector of the line of sight (LOS) (or of $\boldsymbol{r}_R$) has a magnitude equal to the rotation rate and direction along the axis of rotation in the right-hand sense. It can be expressed as

$$\boldsymbol{\Omega}_R = \frac{\boldsymbol{r}_R \times \boldsymbol{V}_R}{r_R^2} \tag{12}$$

where r_R is the length of $\boldsymbol{r}_R$. One can therefore also write

$$\boldsymbol{M} = \frac{r_R^2}{V_R} \boldsymbol{w}_R \times \boldsymbol{\Omega}_R \tag{13}$$

As $\boldsymbol{\Omega}_R \perp \boldsymbol{w}_R$, one gets

$$M = \frac{r_R^2 \Omega_R}{V_R} \tag{14}$$

where Ω_R is the magnitude of $\boldsymbol{\Omega}_R$. Consequently, $\Omega_R = 0$ implies $M = 0$, unless $\boldsymbol{V}_1 = \boldsymbol{V}_2$, and $M = 0$ implies a collision course. This encapsulates the fact that an intruder, converging at constant bearing, is on a collision course. Evidently, $(\boldsymbol{V}_R, \boldsymbol{\Omega}_R, \boldsymbol{M})$ form an orthogonal right-hand system, which it is useful to visualize.

The following lemmas are the foundation of later results about EMD guidance. One can think of $M(\boldsymbol{r}_R, \boldsymbol{V}_R)$ as a scalar function of the two vector fields $\boldsymbol{r}_R$ and $\boldsymbol{V}_R$ (as in the kinetic theory of gases or plasmas). Vector gradients with respect to the fields are denoted by $\partial/\partial \boldsymbol{r}_R$ and $\partial/\partial \boldsymbol{V}_R$ respectively, and $\dot{r}_R$ denotes the time derivative of r_R. It is assumed that $M \neq 0$, and conditions of regularity, such as existence of derivatives, are tacitly assumed.

Lemma 1.

$$\frac{\partial}{\partial \boldsymbol{r}_R} M = \boldsymbol{m} \tag{15}$$

Proof. Taking the vector gradient of Eq. (11) with respect to $\boldsymbol{r}_R$ gives

$$2M \frac{\partial}{\partial \boldsymbol{r}_R} M = 2\boldsymbol{r}_R - 2\frac{\boldsymbol{r}_R \cdot \boldsymbol{V}_R}{V_R^2} \boldsymbol{V}_R = 2\boldsymbol{M} \tag{16}$$

from which the Lemma follows. This Lemma is also the basis of Zeghal's form of the guidance law [30]. □

Lemma 2.

$$\frac{\partial}{\partial \boldsymbol{V}_R} M = -\frac{r_R \dot{r}_R}{V_R^2} \boldsymbol{m} \tag{17}$$

Proof. Taking the vector gradient of Eq. (11) with respect to $\boldsymbol{V}_R$ gives

$$2M \frac{\partial}{\partial \boldsymbol{V}_R} M = -\frac{2(\boldsymbol{r}_R \cdot \boldsymbol{V}_R)\boldsymbol{r}_R}{V_R^2} + \frac{(\boldsymbol{r}_R \cdot \boldsymbol{V}_R)^2}{V_R^2} \frac{2\boldsymbol{V}_R}{V_R^2} = -2\frac{\boldsymbol{r}_R \cdot \boldsymbol{V}_R}{V_R^2} \boldsymbol{M} \tag{18}$$

Differentiating $r_R^2 = \boldsymbol{r}_R \cdot \boldsymbol{r}_R$, one gets

$$r_R \dot{r}_R = \boldsymbol{r}_R \cdot \boldsymbol{V}_R \tag{19}$$

from which the Lemma follows. This Lemma is also the basis of Theorem 10 in Sec. XII, concerning the cockpit display [31]. □

Lemma 3.

$$\dot{M} = -\frac{r_R \dot{r}_R}{V_R^2} \boldsymbol{m} \cdot \dot{\boldsymbol{V}}_R \tag{20}$$

Proof. The time derivative of $M(\boldsymbol{r}_R, \boldsymbol{V}_R)$ can be written

$$\dot{M} = \boldsymbol{V}_R \cdot \frac{\partial}{\partial \boldsymbol{r}_R} M + \dot{\boldsymbol{V}}_R \cdot \frac{\partial}{\partial \boldsymbol{V}_R} M \tag{21}$$

From Eq. (7) one has $\boldsymbol{m} \cdot \boldsymbol{V}_R = 0$. Then Lemmas 1 and 2 give Lemma 3. This Lemma is the basis of Theorem 1 in Sec. V. □

IV. EMD Guidance as Newtonian Dynamics

Before analyzing EMD guidance, some analogies are mentioned to clarify the mathematical context. It is useful to think of the motion as a form of Newtonian two-body dynamics by interpreting $\boldsymbol{a}_i$ as the force exerted on aircraft i by the other aircraft. This implies that both aircraft have a notional unit mass, though their real masses can be different. The force is much more complex than typical interpoint force laws. When written out explicitly, it involves quintuple vector products, originating from Eqs. (1) and (7). Like a magnetic force (the Biot–Savart law), it is not a central force, in that it is not directed along $\boldsymbol{r}_R$. Moreover, $\boldsymbol{a}_1 \neq -\boldsymbol{a}_2$, in general, which violates Newton's third law, and so the centroid of the two aircraft does not have a constant velocity vector [33]. For forces in which the third law holds and the forces are central, the motion of each body is planar in the center-of-mass frame [33] and is therefore easily analyzed. This simplification does not apply here, and the motion is essentially 3-dimensional. Galilean invariance is common in Newtonian dynamics, but does not hold here because absolute velocities appear in $\bar{\boldsymbol{m}}_i$. This reflects the fact that the aircraft are interacting with their environment to achieve their velocities.

The effective force between aircraft is not always repulsive. Figure 1 illustrates a case in which $\boldsymbol{r}_R \cdot \boldsymbol{a}_2 < 0$ initially, and so aircraft 2 feels a component of force of attraction toward aircraft 1, and guides it to turn behind aircraft 1. Also, $\boldsymbol{r}_R \cdot \boldsymbol{a}_1 < 0$, and so aircraft 1 feels a repulsive component of force. This combination achieves effective evasion without excessive turning, which is a very attractive feature of the guidance law. These unusual features of the forces imply that the dynamics depart somewhat from typical 2-body dynamics [33]. The force analogy is intuitive and used frequently here, but the command acceleration is really the basic concept.

The paradox posed by this model is that the force law appears to be very complex and intractable, whereas its geometric basis is relatively simple and natural. After Sec. V, some reformulations related to differential geometry provide some simpler expressions for the guidance law. Then some of its natural properties are revealed.

V. Variation of EMD and Separation with Time

The relative motion of the two aircraft is of central interest. This section describes some basic general features of the variation of M and r_R with time under EMD guidance, illustrated in Fig. 3. First, it is proved that two closing aircraft always steer to improve EMD. In this sense, EMD guidance is effective and achieves its basic objective.

Theorem 1. If two aircraft perform EMD guidance, then

$$\dot{M} = -\frac{r_R \dot{r}_R}{V_R^2} (f_1 |\bar{\boldsymbol{m}}_1|^2 + f_2 |\bar{\boldsymbol{m}}_2|^2) \tag{22}$$

Hence, M increases when r_R decreases and decreases when r_R increases, until $M = 0$.

Proof. From the guidance equations (4), one gets

$$\boldsymbol{m} \cdot \dot{\boldsymbol{V}}_1 = -f_1 \boldsymbol{m} \cdot (\boldsymbol{u}_1 \times \boldsymbol{m} \times \boldsymbol{u}_1) = -f_1 |\boldsymbol{m} \times \boldsymbol{u}_1|^2 = -f_1 |\bar{\boldsymbol{m}}_1|^2 \tag{23}$$

Similarly, one gets $\boldsymbol{m} \cdot \dot{\boldsymbol{V}}_2 = f_2 |\bar{\boldsymbol{m}}_2|^2$, and so

$$\boldsymbol{m} \cdot \dot{\boldsymbol{V}}_R = f_1 |\bar{\boldsymbol{m}}_1|^2 + f_2 |\bar{\boldsymbol{m}}_2|^2 \tag{24}$$

Then Lemma 3 implies the Theorem. □

After CPA, EMD relates to a hypothetical past encounter, and so a decreasing M indicates an improving situation.

Another major point of interest is the general variation of r_R with time. The CPA is a stationary point (SP) of the motion in the sense that $\dot{r}_R = 0$. From Eq. (19), one gets

$$\boldsymbol{r}_R \cdot \boldsymbol{V}_R = 0 \tag{25}$$

at an SP. Thus, Eq. (9) implies

$$\boldsymbol{M} = \boldsymbol{r}_R \tag{26}$$

at an SP, for any guidance law or motion. Equations (12) and (25) imply that $\boldsymbol{r}_R$, $\boldsymbol{V}_R$, and $\boldsymbol{\Omega}_R$ are mutually orthogonal at the CPA, which it is useful to visualize. The following Theorem shows that r_R always decreases down to a unique CPA and subsequently increases. This is very desirable behavior, but, because the forces are sometimes attractive, it is not at all obvious that it holds.

Theorem 2. If two aircraft perform EMD guidance, then the forces both have a repulsive component at any stationary point of r_R, and so $\ddot{r}_R \geq 0$. Hence, the CPA is the unique local minimum of r_R.

Proof. Equation (26) implies that, at an SP,

$$\dot{\boldsymbol{V}}_1 = -\frac{f_1}{r_R}\boldsymbol{u}_1 \times \boldsymbol{r}_R \times \boldsymbol{u}_1 \tag{27}$$

which gives

$$\boldsymbol{r}_R \cdot \dot{\boldsymbol{V}}_1 = -\frac{f_1}{r_R}|\boldsymbol{r}_R \times \boldsymbol{u}_1|^2 \leq 0 \tag{28}$$

Similarly,

$$\boldsymbol{r}_R \cdot \dot{\boldsymbol{V}}_2 = \frac{f_2}{r_R}|\boldsymbol{r}_R \times \boldsymbol{u}_2|^2 \geq 0 \tag{29}$$

which proves that both forces have a repulsive component. Differentiating Eq. (19) gives

$$\ddot{r}_R = \frac{1}{r_R}(V_R^2 - \dot{r}_R^2 + \boldsymbol{r}_R \cdot \dot{\boldsymbol{V}}_R) \tag{30}$$

In general, $V_R^2 \geq \dot{r}_R^2$, and obviously so at an SP. Also,

$$\boldsymbol{r}_R \cdot \dot{\boldsymbol{V}}_R = \boldsymbol{r}_R \cdot \dot{\boldsymbol{V}}_2 - \boldsymbol{r}_R \cdot \dot{\boldsymbol{V}}_1 \geq 0 \tag{31}$$

and so $\ddot{r}_R \geq 0$. It follows that $r_R(t)$ has no local maximum, and so it has, at most, one local minimum, which is the CPA. This completes the proof. □

An immediate consequence of Theorems 1 and 2 is that $M(t)$ has a unique maximum, occurring at the CPA, which shows that the guidance law achieves its basic objective. In Fig. 2, both forces are evidently strictly repulsive at the CPA. Hence, there is a transition point before CPA at which the force on aircraft 2 first becomes repulsive.

A notable property of EMD guidance is that it reaches a natural termination point beyond which there are no accelerations, even if the force coefficients have infinite range. This contrasts sharply with other common force laws. The basic result is as follows.

Theorem 3. If two aircraft perform EMD guidance and the quantities $f_i r_R$ are uniformly bounded away from zero, then (after CPA) M falls to zero in a finite time.

Proof. The main condition means that $f_i r_R \geq C$ for all r_R, where C is a (strictly) positive constant. As just noted, M can only decrease after CPA. Suppose the Theorem were false. Then M would tend to a nonnegative limit as $t \to \infty$. Hence, $\dot{M}$ would tend to zero, and so the right side of Eq. (22) would tend to zero. By Theorem 2, $\dot{r}_R \neq 0$ in the limit. Also, V_R is bounded above by the constant $V_1 + V_2$. It would therefore follow from Eq. (22) that $|\bar{\boldsymbol{m}}_1| \to 0$ and $|\bar{\boldsymbol{m}}_2| \to 0$. These imply that $\boldsymbol{m} \| \boldsymbol{u}_1 \| \boldsymbol{u}_2$ in the limit, which in turn implies that $\boldsymbol{m} \| \boldsymbol{V}_R$ in the limit. However, $\boldsymbol{m} \perp \boldsymbol{V}_R$ in general. These are inconsistent, because V_R is not zero in the limit (and obviously never zero if $V_1 \neq V_2$). This contradiction refutes the supposition that the Theorem is false, which completes the proof. □

It is sufficient that the f_i decay no faster than $1/r_R$, which might seem incongruous. It suggests that longer range f_i cause M to fall more quickly to zero. This is confirmed when examples using constant f_i are compared with examples using f_i from Eq. (6). However, the Theorem does not say that such a condition is necessary, and a stronger version of the Theorem would be useful.

When M falls to 0, we define the $\boldsymbol{a}_i$ to be zero. This is termed the ultimate point of escape (UPE). Thereafter, the aircraft recede along straight paths radiating from a past extrapolated collision point (Fig. 2). As collision points are be avoided, there is an underlying logical principle influencing the ultimate paths. Then $\boldsymbol{\Omega}_R = \boldsymbol{0}$, and the paths are obviously coplanar.

The guidance equations (4) are time-reversal-invariant, meaning that they do not change if t is replaced by $-t$ and each $\boldsymbol{V}_i$ is replaced by $-\boldsymbol{V}_i$. Thus, the reversed motion obeys the same EMD guidance. Hence, for any initial state with $M \neq 0$, Theorem 3 implies that there is an earlier hypothetical time $t_0 < 0$ (when $M = 0$), which evolves into the given initial state. The time t_0 is called the earliest point of guidance (EPG).

Theorems 1 to 3 provide a basic qualitative picture of the variation of r_R and M for general f_i and show that EMD guidance produces motion that may be properly described as evasive. One can check that Fig. 3 is consistent with the preceding theorems.

VI. Classification of Turning Directions Under EMD Guidance

This section gives a simple general classification of the turning directions of aircraft, resulting from EMD guidance, in terms of the turning direction of the LOS. It also shows how to manage cases in which $M = 0$ initially, as foreshadowed after Eqs. (4). The instantaneous response of an aircraft has been expressed in terms of the lateral acceleration $\boldsymbol{a}_i$, in common with other real-time guidance laws. Aspects of the motion can be analyzed and understood better in terms of the angular velocity vectors of the aircraft. This reformulation, mentioned in Sec. IV, is related to the differential geometry of the space curves formed by the paths of the aircraft [34].

The unit vector along the velocity vector $\boldsymbol{V}_i$ of aircraft i is denoted as $\boldsymbol{u}_i$. This is also the tangent vector to the path. Then the angular velocity vector of $\boldsymbol{u}_i$ is

$$\Gamma_i = \boldsymbol{u}_i \times \dot{\boldsymbol{u}}_i \tag{32}$$

Thus, $|\Gamma_i|$ is V_i times the curvature of the path [34]. Because $\boldsymbol{a}_i = \Gamma_i \times \boldsymbol{V}_i$ and $\boldsymbol{u}_i$, $\boldsymbol{a}_i$, and Γ_i are mutually orthogonal, one has

$$\Gamma_i = \frac{\boldsymbol{V}_i \times \boldsymbol{a}_i}{V_i^2} \tag{33}$$

which is an analog of Eq. (12). Substituting from Eqs. (2) and (3), one gets

$$\Gamma_1 = \frac{f_1}{V_1}\boldsymbol{m} \times \boldsymbol{u}_1, \qquad \Gamma_2 = -\frac{f_2}{V_2}\boldsymbol{m} \times \boldsymbol{u}_2 \tag{34}$$

These evidently have a simpler form than the accelerations in Eqs. (2) and (3).

The directions in which the aircraft turn can be related to the direction of rotation of the LOS. Such a relationship is natural for pilots with intuition based on "see and avoid." Substituting Eq. (13) in Eq. (34) and using Eq. (14) gives

$$\Gamma_1 = \frac{f_1 r_R^2}{V_1 M V_R}(\boldsymbol{w}_R \times \boldsymbol{\Omega}_R) \times \boldsymbol{u}_1 = \frac{f_1}{V_1}(\boldsymbol{o}_R \boldsymbol{u}_1 \cdot \boldsymbol{w}_R - \boldsymbol{o}_R \cdot \boldsymbol{u}_1 \boldsymbol{w}_R) \tag{35}$$

where $\boldsymbol{o}_R = \boldsymbol{\Omega}_R / |\boldsymbol{\Omega}_R|$ is the unit vector along the axis of rotation of the LOS. Similarly,

$$\Gamma_2 = \frac{f_2}{V_2}(-\boldsymbol{o}_R \boldsymbol{u}_2 \cdot \boldsymbol{w}_R + \boldsymbol{o}_R \cdot \boldsymbol{u}_2 \boldsymbol{w}_R) \tag{36}$$

Because $\boldsymbol{\Omega}_R \perp \boldsymbol{w}_R$, one gets

$$\Gamma_1 \cdot \boldsymbol{o}_R = \frac{f_1}{V_1}\boldsymbol{u}_1 \cdot \boldsymbol{w}_R \tag{37}$$

Now,

$$\boldsymbol{u}_1 \cdot \boldsymbol{w}_R = \frac{\boldsymbol{V}_1 \cdot \boldsymbol{V}_R}{V_1 V_R} = \frac{\boldsymbol{V}_1 \cdot \boldsymbol{V}_2 - V_1^2}{V_1 V_R} \tag{38}$$

If $V_1 > V_2$, then the numerator is less than $\boldsymbol{V}_1 \cdot \boldsymbol{V}_2 - V_1 V_2 \leq 0$, and so $\Gamma_1 \cdot \boldsymbol{o}_R < 0$. Thus, the rotation of the faster aircraft is opposite to the rotation of the LOS. In general, one can write

$$\Gamma_1 \cdot \boldsymbol{o}_R = \frac{f_1}{V_R}\left(\frac{V_2}{V_1}\cos\phi_R - 1\right) \tag{39}$$

where $\phi_R > 0$ is the angle between $\boldsymbol{V}_1$ and $\boldsymbol{V}_2$. Thus, $\Gamma_1 \cdot \boldsymbol{o}_R < 0$ if ϕ_R is obtuse or if the speeds are equal. Similarly,

$$\Gamma_2 \cdot \boldsymbol{o}_R = -\frac{f_2}{V_2}\boldsymbol{u}_2 \cdot \boldsymbol{w}_R = \frac{f_2}{V_R}\left(\frac{V_1}{V_2}\cos\phi_R - 1\right) \tag{40}$$

The results are now summarized and illustrated in Fig. 4 with a fixed $\phi_R = 55$ deg.

Theorem 4. Suppose two aircraft perform EMD guidance:

1) If $\cos\phi_R > V_1/V_2$, then $\Gamma_1 \cdot \boldsymbol{o}_R > 0$ and $\Gamma_2 \cdot \boldsymbol{o}_R < 0$.

2) If $\cos\phi_R > V_2/V_1$, then $\Gamma_1 \cdot \boldsymbol{o}_R < 0$ and $\Gamma_2 \cdot \boldsymbol{o}_R > 0$.

3) Otherwise, $\Gamma_1 \cdot \boldsymbol{o}_R < 0$ and $\Gamma_2 \cdot \boldsymbol{o}_R < 0$.

For planar motion, all the angular velocity vectors are normal to the plane. Then Eqs. (35) and (36) reduce to

$$\Gamma_1 = \frac{f_1 \boldsymbol{u}_1 \cdot \boldsymbol{w}_R}{V_1}\boldsymbol{o}_R, \qquad \Gamma_2 = -\frac{f_2 \boldsymbol{u}_2 \cdot \boldsymbol{w}_R}{V_2}\boldsymbol{o}_R \tag{41}$$

Thus, the Theorem provides a complete set of turning rules for planar motion. This generalizes the results in [31], in which examples of turning according to EMD guidance were shown to be more effective than the basic rules of the air for conflict situations. If aircraft 2 is replaced by a fixed obstacle, as in the example of Sec. II, then Eq. (41) reduces to

$$\Gamma_1 = -\frac{f_1}{V_1}\boldsymbol{o}_R \tag{42}$$

Then turning is always opposed to the rotation of the LOS. Moreover, if f_1 is constant, the aircraft follows a circular arc of radius V_1^2/f_1, as mentioned after Eq. (5).

Force coefficients f_i need not be isotropic functions, and so the magnitudes of Γ_i could depend on the 3-D orientation of the maneuvers. This would distinguish between horizontal and vertical maneuvers, especially in less agile aircraft. The specific form of each f_i could depend on the performance details of the aircraft.

As noted after Eqs. (4), if $M = 0$ initially, then guidance is not defined and must be carefully initiated. Equations (35) and (36) are better conditioned in this case, because M has been divided out. However, $\boldsymbol{\Omega}_R = \boldsymbol{0}$ here, and so $\boldsymbol{o}_R$ is not defined. For planar motion, either normal to the plane may be chosen for $\boldsymbol{o}_R$. Equation (41) shows that the two alternatives produce motions that are just mirror images. For 3-D motion, $M = 0$ implies that the motion is instantaneously planar. If an initiating $\boldsymbol{o}_R^0$ is chosen normal to the plane, then planar motion ensues, as previously noted. If $\boldsymbol{o}_R^0$ is chosen in the plane, then out-of-plane motion is accentuated. Other choices are possible, subject to $\boldsymbol{o}_R^0$ being normal to $\boldsymbol{w}_R$, to be consistent with Eq. (12). The choice of $\boldsymbol{o}_R^0$ might be influenced by the practical factors mentioned at the end of Sec. II. Once the true $\boldsymbol{o}_R$ is well defined, in the presence of noise, EMD guidance can be invoked.

VII. Geometric Description of the Paths of Interchangeable Aircraft

In 3-D, the paths have twisting, intertwining forms that are difficult to visualize and describe. An understanding of these forms can be built up by looking at their basic geometric properties. These properties can be inferred from the guidance law as follows. Note the appearance of similarity and symmetry of the paths in Fig. 2. Here, it is shown that this is a consequence of choosing $f_1 = f_2$ and $V_1 = V_2$. Then, if the labels 1 and 2 are exchanged in the differential equations (4), the equations themselves are exchanged, and so the system of equations is unchanged or invariant. In this sense, the two aircraft are equivalent or interchangeable. The restriction to interchangeable aircraft is limiting from a practical point of view, but has potential application when speeds are set by regulation, convention, or linked controls, especially if the aircraft are similar.

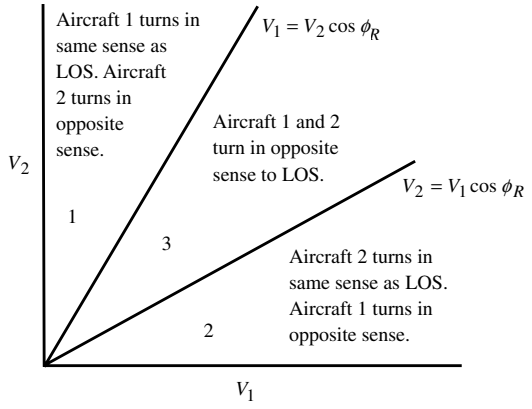

Fig. 4 Illustration of the turning directions resulting from EMD guidance.

We shall also consider a force coefficient that is an isotropic function. This implies that horizontal and vertical maneuvers are treated equally. It is appropriate for spacecraft and reasonable for very agile aircraft, but might be less suitable for large aircraft. Equation (6) is an example of an isotropic force coefficient. A more general example is a function of the scalar variables r_R, M, and V_R describing the relative situation. The term isotropic EMD guidance is used here.

Isotropic force coefficients ensure that the guidance equations (4) have a vector-invariant form and are therefore invariant under Euclidean transformations (translations and rotations) [33]. We single out those Euclidean transformations that involve proper rotations, excluding reflections. These are the so-called rigid-body transformations. One needs to distinguish between the groups $E^+(2)$ and $E^+(3)$ of such transformations in 2-D and 3-D, respectively. For example, if p, q, and d are regarded as objects, then p $\equiv$ q in $E^+(3)$, but not in $E^+(2)$, whereas p $\equiv$ d in $E^+(2)$ and hence in $E^+(3)$. Congruence ($\equiv$) here means identity under such transformations.

Theorem 5. Suppose that the aircraft are interchangeable in isotropic EMD guidance. Then between EPG and UPE,

1) The two paths are congruent in $E^+(3)$.

2) For planar motion, the paths are mirror-congruent in $E^+(2)$.

In both cases, when the two paths are brought into coincidence, the reversed motion on one path coincides with the forward motion on the other.

Mirror-congruent means the mirror image of one is congruent to the other. Statement 2 is consistent with statement 1, for p and q are mirror images in $E^+(2)$ and p $\equiv$ q in $E^+(3)$. Another way of stating the Theorem is to associate a direction with a path. Then statement 1 could be expressed as follows: the backward path of one aircraft, from UPE to EPG, is congruent in $E^+(3)$ to the forward path of the other aircraft, from EPG to UPE.

Proof 1. One can construct a proof by starting with any initial conditions and performing a sequence of transformations that restore the initial conditions before interchange. However, the following method is simpler and clearer. The paths may be continued unchanged, beyond any time t, by taking the current state as the initial state. As mentioned after Theorem 3, Eqs. (4) are also time-reversal-invariant (TRI). Hence, the paths before t are simply retraced if the conditions at t are reversed. Now choose the current time at the CPA. From Eq. (25), $\boldsymbol{r}_R \cdot \boldsymbol{V}_R = 0$ at the CPA (for any motion), and so the velocity vectors make equal angles with the LOS. First suppose that the velocity vectors are not parallel at the CPA, as is usual. To accommodate planar motion, the configuration is drawn as in Fig. 5. The plane of the page is chosen to contain $\boldsymbol{r}_R$ and $\boldsymbol{V}_1$. In general, $\boldsymbol{V}_2$ will not lie in this plane. It is chosen to be inclined out of the page in this instance, as indicated by the circular arrowhead symbol.

TRI implies that the velocities may be reversed without affecting the paths, as in Fig. 6. Here, the circular arrow tail indicates that $-\boldsymbol{V}_2$ is inclined into the page. For 3-D motion, $E^+(3)$ invariance of the

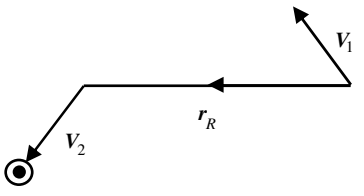

Fig. 5 The initial state.

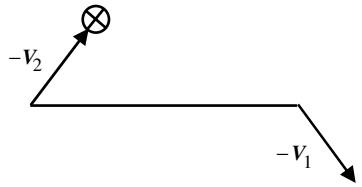

Fig. 6 Reversed initial conditions.

paths allows a rotation about an axis lying in the page and normal to the LOS, without affecting the paths, resulting in Fig. 7. A rotation about the LOS results in Fig. 8.

Interchangeability allows an exchange of labels without affecting the paths. This reproduces Fig. 5, which proves the congruence. If the velocity vectors were parallel in Fig. 5, then they would be normal to the LOS, as Eq. (25) shows. Then the proof would be trivial. (Theorem 7 shows that V_R is not zero at the CPA, and so this case does not arise in EMD guidance.) This completes proof 1 of Theorem 5. □

Proof 2. In 2-D, the vectors are coplanar, and so the circular arrow heads and tails are omitted. The rotations leading to Figs. 7 and 8 are not possible in $E^+(2)$. Instead, Fig. 6 is reflected across a line on the page and normal to the LOS, producing Fig. 9. An exchange of labels reproduces Fig. 5, which completes proof 2 of Theorem 5. □

The symmetric forms of $r_R(t)$ and $M(t)$ in Fig. 3 are related to the symmetry of the paths, as follows.

Corollary 5.1. If the aircraft are interchangeable in isotropic EMD guidance, then $r_R(t), M(t), V_R(t)$, and $\Omega_R(t)$ are symmetric in t about the CPA.

Proof. These variables are invariant under interchange of labels and Euclidean transformations. Figures 5–9 show that the motion after CPA matches the reversed motion before CPA, which proves the result. □

In fact, V_R is constant, as Theorem 7 shows. Then Eq. (14) and Theorems 1 and 2 show that $\Omega_R(t)$ has a maximum and a turning point at the CPA.

A 3-D path is a smooth space curve, and so its shape is completely described by its curvature and torsion [34]. The curvatures have some general properties. Let $\kappa_i(t)$ denote the curvature of path i at time t.

Theorem 6. If the aircraft are interchangeable in EMD guidance, then the two paths have equal curvatures at any instant of time:

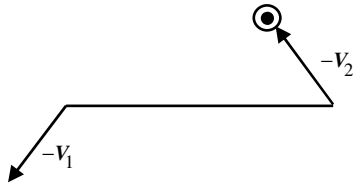

Fig. 7 Rotation normal to LOS.

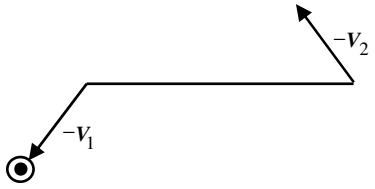

Fig. 8 Rotation about LOS.

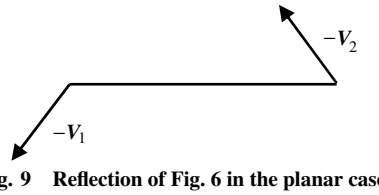

Fig. 9 Reflection of Fig. 6 in the planar case.

$$\kappa_1(t) = \kappa_2(t) \tag{43}$$

Proof. Now f and V denote the common values of f_i and V_i. From Eq. (34), one gets

$$|\Gamma_1|^2 = \frac{f^2}{V^4}[V^2 - (\boldsymbol{m} \cdot \boldsymbol{V}_1)^2] \tag{44}$$

Because $\boldsymbol{m} \cdot \boldsymbol{V}_R = 0$, this coincides with $|\Gamma_2|^2$. As mentioned $|\Gamma_i| = V\kappa_i$, and so Eq. (43) follows. This implies that the aircraft turn equally hard at any instant, and so, in this sense, they make an equal effort to evade. □

Let $t*$ be the time such that t and $t*$ occur at equal time intervals from CPA on opposite sides. Then statement 1 in Theorem 5 implies that

$$\kappa_1(t*) = \kappa_2(t) \tag{45}$$

for isotropic EMD guidance. When combined with Eq. (43), this gives

$$\kappa_i(t) = \kappa_i(t*) \tag{46}$$

and so the curvature of a path is symmetric about its CPA. A planar path is completely described by its curvature, and so one can draw some immediate conclusions.

Corollary 6.1. Suppose the aircraft are interchangeable in EMD guidance and the motion is planar. Then,

1) The paths are congruent in $E^+(2)$.

2) The path segment of an aircraft up to CPA is a mirror image of the segment beyond CPA.

Proof. Point 1 follows from Eq. (43) and point 2 follows from Eq. (44). □

Figure 10 illustrates the planar case. Paths 1 and 2 have EPG points A_1 and A_2, CPA points B_1 and B_2, and UPE points C_1 and C_2. The arcs A_1B_1, B_1C_1, A_2B_2, and B_2C_2 are of equal duration and hence equal length. By statement 2 in Theorem 5, $A_1B_1 \equiv \overline{C_2B_2}$, where the overbar indicates a mirror image. By Theorem 6, $C_2B_2 \equiv C_1B_1$. Hence, $A_1B_1 \equiv \overline{C_1B_1}$, and so path 1 is symmetric about its normal through B_1. The same holds for path 2. In summary, a reflection of path 1 in the plane normal to the LOS at the CPA maps the reversed motion on path 1 onto the motion on path 2. A path has mirror symmetry across the broken line through its CPA. The EPG and the UPE are symmetrically disposed in time and position relative to the CPA.

In 2-D, one can get a simpler expression for the angular velocity or curvature. As the speeds are equal, one has

$$\boldsymbol{w}_R \cdot \boldsymbol{u}_1 + \boldsymbol{w}_R \cdot \boldsymbol{u}_2 = \frac{V_2^2 - V_1^2}{V_R V} = 0 \tag{47}$$

Hence,

$$\boldsymbol{w}_R \cdot \boldsymbol{u}_1 = -\boldsymbol{w}_R \cdot \boldsymbol{u}_2 = \frac{\boldsymbol{w}_R \cdot (\boldsymbol{u}_1 - \boldsymbol{u}_2)}{2} = -\frac{V_R}{2V} \tag{48}$$

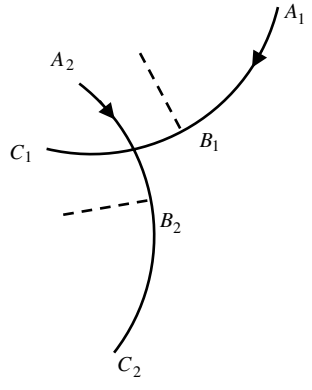

Fig. 10 Symmetry and congruence of planar paths.

Thus, Eq. (41) becomes

$$\Gamma_1 = \Gamma_2 = -\frac{fV_R}{2V^2}\boldsymbol{o}_R \tag{49}$$

For example, if f is constant, then Γ_i are constant, and so both aircraft follow arcs of circles of radius $2V^3/fV_R = V^2/f\sin(\phi_R/2)$, where ϕ_R is the angle between $\boldsymbol{V}_1$ and $\boldsymbol{V}_2$. For strongly converging paths, ϕ_R is large, and so the radius is small. This more severe evasion is a desirable property. For example, if the velocity vectors are oppositely directed, then the radius takes its minimum value V^2/f. The radius and initial directions determine the centers of the circles. Each aircraft feels a force $f\sin(\phi_R/2)$ directed at the center of its circle, as though these were centers of attraction. Further details of the motion are given in Sec. XI.

In 3-D, Eq. (46) implies that a path curvature is symmetric across CPA, but not the path itself, as the example in Fig. 11 illustrates. This is because the path torsions $\tau_i(t)$ are not equal: $\tau_1(t) \neq \tau_2(t)$. So, although statement 1 in Theorem 5 implies $\tau_1(t*) = \tau_2(t)$, one concludes that $\tau_i(t*) \neq \tau_i(t)$.

Consider, however, the very special case in which the initial conditions are symmetric; that is, an exchange of labels followed by a $E^+(3)$ transformation restores the original initial conditions. An example is two converging aircraft for which the velocity vectors make equal internal angles with the LOS (but are not necessarily coplanar with the LOS). Then the two forward paths must be congruent in $E^+(3)$. Hence, statement 1 in Theorem 5 implies that the path segment of an aircraft up to CPA is congruent in $E^+(3)$ to the segment beyond CPA.

Figure 11 is a plan view of the 3-D paths of two interchangeable aircraft with force coefficients in Eq. (6) and $p_1 = p_2 = 0.5$. Again, the units of distance are arbitrary and the paths are independent of the common speed. Aircraft 1 and 2 make angles of 46 and -45 deg with the x axis, and so there is a small asymmetry in the initial conditions. Both aircraft are initially moving horizontally and aircraft 1 is slightly higher (0.03 units), and so the guidance law causes it to climb and aircraft 2 to descend. The aircraft reach a CPA and an UPE and continue on straight paths, as shown in Fig. 11. No congruencies or symmetries are evident in this view.

Figure 12 shows the same paths projected onto the plane normal to the LOS at the CPA, so that $\boldsymbol{r}_R$ points into the page. Here, the x' axis is horizontal and normal to this LOS, whereas the y' axis is normal to the x' axis and the LOS. In this projection, the paths are evidently mirror images in $E^+(2)$, with the line of symmetry indicated. Figure 13 shows the same paths projected onto the plane normal to the line of symmetry. The x'' axis is along the line of symmetry and the y'' axis is along the LOS. In this projection, the paths are also mirror images in $E^+(2)$, with the line of symmetry indicated. Figures 12 and 13 thereby illustrate the congruence in $E^+(3)$ described in statement 1 in Theorem 5.

To digress, note that the proofs of Theorem 5 use only the invariance properties of the guidance equations (4), and so they apply to other guidance or two-body dynamics with such properties. Also note that the symmetries are analogs of important symmetries in fundamental particle physics. Interchange of labels is a form of conjugation (operator C), reflection changes the parity of a curve (operator P), and time reversal is an operator T. Then, for example, statement 2 in Theorem 5 expresses the CPT invariance of paths in $E^+(2)$.

VIII. Detailed Properties for Interchangeable Aircraft

For interchangeable aircraft, one can obtain simple representations of the angular velocity vectors, which help to explain the shapes of the paths as seen in their different projections. The motion also has some remarkable features, such as the following.

Theorem 7. If the aircraft are interchangeable in EMD guidance, then V_R is constant. Equivalently, the angle ϕ_R between $\boldsymbol{V}_1$ and $\boldsymbol{V}_2$ remains fixed. Equivalently, the centroid moves at constant speed.

Proof. Equations (4) imply

$$\dot{\boldsymbol{V}}_R = f(\bar{\boldsymbol{m}}_1 + \bar{\boldsymbol{m}}_2) = f(2\boldsymbol{m} - \boldsymbol{m}\cdot\boldsymbol{u}_1\boldsymbol{u}_1 - \boldsymbol{m}\cdot\boldsymbol{u}_2\boldsymbol{u}_2) \tag{50}$$

In general, $\boldsymbol{m}\cdot\boldsymbol{V}_R = 0$, which implies

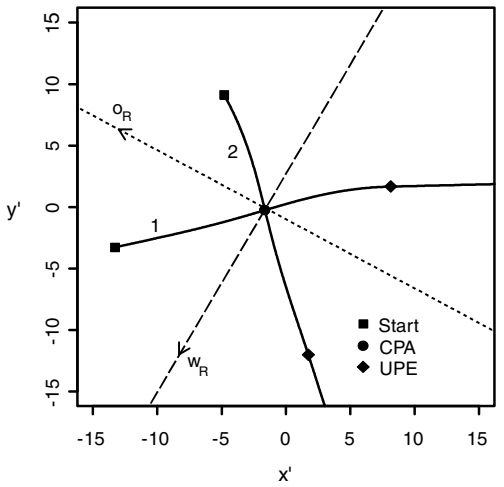

Fig. 12 The paths of Fig. 11 projected onto the plane normal to the LOS at the CPA. The projections are mirror images across the dashed line.

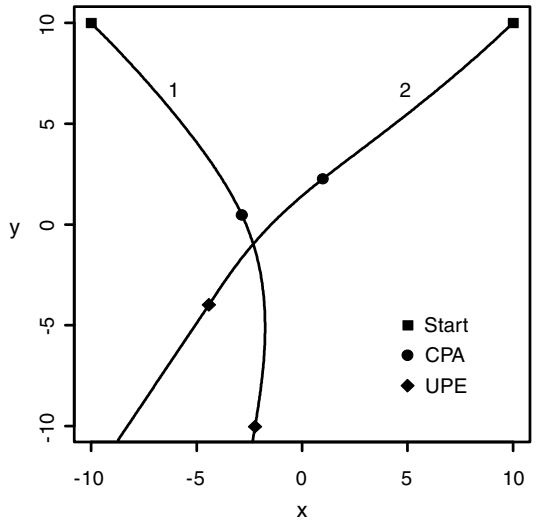

Fig. 11 Plan view of the 3-D motion of two aircraft. Aircraft 1 turns upward (out of the page) and aircraft 2 turns downward.

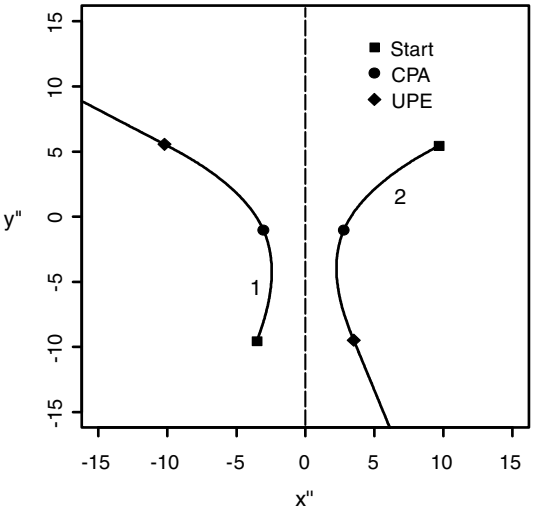

Fig. 13 The paths of Figs. 11 and 12 projected onto the plane containing the LOS at the CPA and the line of symmetry in Fig. 12.

$$\boldsymbol{m} \cdot \boldsymbol{u}_1 = \boldsymbol{m} \cdot \boldsymbol{u}_2 = \boldsymbol{m} \cdot \bar{\boldsymbol{u}} \tag{51}$$

where

$$\bar{\boldsymbol{u}} = \tfrac{1}{2}(\boldsymbol{u}_1 + \boldsymbol{u}_2) \tag{52}$$

This implies

$$\dot{\boldsymbol{V}}_R = 2f(\boldsymbol{m} - \boldsymbol{m} \cdot \bar{\boldsymbol{u}}\, \bar{\boldsymbol{u}}) \tag{53}$$

Then

$$V_R \dot{V}_R = \boldsymbol{V}_R \cdot \dot{\boldsymbol{V}}_R = 2f(\boldsymbol{m} \cdot \boldsymbol{V}_R - \boldsymbol{m} \cdot \bar{\boldsymbol{u}}\, \bar{\boldsymbol{u}} \cdot \boldsymbol{V}_R) \tag{54}$$

Both terms on the right side are zero, and so V_R is constant. The centroid has speed $\sqrt{V^2 - V_R^2/4}$, which is therefore constant. This completes the proof. □

As mentioned, the velocity vector of the centroid is not constant, because Newton's third law does not hold for the forces.

For planar motion, a constant of ϕ_R is consistent with statement 2 in Theorem 5 and with the equal angular velocities in Eq. (49). In 3-D, a constant ϕ_R means that, as viewed by one aircraft (which sees its path as a fixed axis), the other aircraft follows a helix of a general type [34]. This intertwining motion is clarified further as follows.

Theorem 8. If the aircraft are interchangeable in EMD guidance, then

$$\Gamma_1 = -G\boldsymbol{o}_R - H\boldsymbol{w}_R \tag{55}$$

$$\Gamma_2 = -G\boldsymbol{o}_R + H\boldsymbol{w}_R \tag{56}$$

where

$$G = \frac{fV_R}{2V^2} > 0, \qquad H = \frac{f\boldsymbol{o}_R \cdot \bar{\boldsymbol{V}}}{V^2} \tag{57}$$

and $\bar{\boldsymbol{V}}$ is the velocity vector of the centroid. Hence, the aircraft turn equally about $-\boldsymbol{o}_R$ and oppositely about $\boldsymbol{w}_R$.

Proof. In general, $\boldsymbol{o}_R \cdot \boldsymbol{w}_R = 0$, and so in this case,

$$\boldsymbol{o}_R \cdot \boldsymbol{u}_1 = \boldsymbol{o}_R \cdot \boldsymbol{u}_2 = \boldsymbol{o}_R \cdot \bar{\boldsymbol{V}}/V \tag{58}$$

Also, $\bar{\boldsymbol{V}} \cdot \boldsymbol{V}_R = 0$, and so $\boldsymbol{V}_2 \cdot \boldsymbol{V}_R = -\boldsymbol{V}_1 \cdot \boldsymbol{V}_R = V_R^2/2$. Thus,

$$\boldsymbol{u}_2 \cdot \boldsymbol{w}_R = -\boldsymbol{u}_1 \cdot \boldsymbol{w}_R = V_R/2V \tag{59}$$

Putting Eqs. (58) and (59) in Eqs. (35) and (36) gives the equations of the Theorem. The motion lies in class 3 of Fig. 4. □

Because $\boldsymbol{r}_R \perp \boldsymbol{o}_R$, in general, and $\boldsymbol{r}_R \perp \boldsymbol{w}_R$ at the CPA, it follows that $\Gamma_i \perp \boldsymbol{r}_R$ at the CPA, and so Γ_i have no component along $\boldsymbol{r}_R$. In Fig. 12, this is manifested as points of inflexion in the projected paths at the CPA. It also means that the turns lie in the most effective planes, away from the LOS, at the CPA.

The Theorem confirms that $|\Gamma_1| = |\Gamma_2|$, in accordance with Eq. (44). Equations (55) and (56) show that $\boldsymbol{w}_R$ at the CPA is the axis of symmetry in Figs. 12 and 13, indicated by the dashed line. Then Eq. (12) implies that $\boldsymbol{o}_R$ is the normal in Fig. 12, indicated by the dotted line.

For the initial state in Fig. 11, $\boldsymbol{o}_R$ is vertical and $\boldsymbol{w}_R$ is horizontal. Both aircraft turn right at rate G, aircraft 1 turns upward at rate H, and aircraft 2 turns downward at rate H, causing the LOS to rotate. At any later time, $\boldsymbol{o}_R$ is not vertical, but let it define a new vertical and a new horizontal plane. Therein the turn rates are the current G and H, and so the rotation of the LOS continues in a screw motion.

IX. When Only One Aircraft Evades

Aircraft 2 will not evade if $f_2 = 0$, but will continue with a constant velocity vector. This would apply if it is unaware or uncooperative. Theorems 1 and 2 hold in this case, and so the evasive action of aircraft 1 is effective in the same way. More generally, the motion of aircraft 2 might be quite arbitrary. Then Eq. (22) is replaced by

$$\dot{M} = -\frac{r_R \dot{r}_R}{V_R^2}(\boldsymbol{m} \cdot \dot{\boldsymbol{V}}_2 + f_1 |\bar{\boldsymbol{m}}_1|^2) \tag{60}$$

The first term is just the value of $\dot{M}$ when $\dot{\boldsymbol{V}}_1 = \boldsymbol{0}$: that is, when 1 does not evade. The second term is positive while the aircraft are closing. This implies the following Theorem.

Theorem 9. If aircraft 2 does not evade or has arbitrary motion, EMD guidance by aircraft 1 increases M faster than subsequent steady motion by aircraft 1. In this sense, EMD guidance is effective when only one aircraft evades.

X. Geometric Formulation of EMD Guidance Equations

For one class of EMD guidance, as illustrated in Figs. 2 and 11, a path has the same shape for all speeds: that is, a path remains geometrically self-similar. Thus, the two paths may be applied to different types of aircraft or other vehicles after a change of distance scale. To show this, one defines a curvature vector $\boldsymbol{K}_1$ for which the magnitude is the curvature of path 1 and for which the direction is along the axis of rotation of the tangent vector in the right-hand sense (though [34] assigns a different direction). Then $\Gamma_1 = V_1 \boldsymbol{K}_1$, and for the force coefficients of Eq. (6), Eq. (34) becomes

$$\boldsymbol{K}_1 = \frac{p_1}{r_R}\boldsymbol{m} \times \boldsymbol{u}_1, \qquad \boldsymbol{K}_2 = -\frac{p_2}{r_R}\boldsymbol{m} \times \boldsymbol{u}_2 \tag{61}$$

If $V_1 = V_2$, then Eq. (7) implies that $\boldsymbol{m}$ does not depend on the speed, and so neither do the curvatures and, consequently, neither do the paths. In this case, the motion of the aircraft does not play an essential role. Rather, Eq. (61) combined with initial positions and directions are defining equations for two space curves in differential geometry, with pairs of points associated. The case in which 2 is a fixed obstacle illustrates this rather clearly. Then Eq. (42) becomes

$$\boldsymbol{K}_1 = \frac{p_1}{r_R}\boldsymbol{o}_R \tag{62}$$

which shows that the local radius of curvature of path 1 is just a fixed multiple of the radial distance from the obstacle.

XI. Exact Solutions for Planar Motion with Separation Control and Turning Limits

This section provides exact solutions for the planar motion of two interchangeable aircraft and for an aircraft avoiding a fixed obstacle. This provides much explicit detail about the motion. It also provides control over the minimum separation and accommodates limits on the turning capability of the aircraft.

For two interchangeable aircraft, the equality of the angular velocities [Eq. (34)], proved in Theorem 6, implies that $|\bar{\boldsymbol{m}}_1| = |\bar{\boldsymbol{m}}_2|$. For planar motion, Eq. (49) implies that these have value $V_R/2V$. Putting this in Eq. (22) gives

$$\dot{M} = -\frac{fr_R \dot{r}_R}{2V^2} \tag{63}$$

If f is a constant, where the paths are equal circles [Eq. (49)], then $M + fr_R^2/4V^2$ is a constant of the motion. The separation $\bar{r}_R$ at the CPA, where $r_R = M$, is therefore given by a quadratic equation. Conversely, to exceed a given $\bar{r}_R$, one requires

$$f > \frac{4V^2[\bar{r}_R - M(0)]}{r_R(0)^2 - \bar{r}_R^2} \tag{64}$$

If $r_R(0) > \bar{r}_R$, then, without further constraints, a nominated safe separation $\bar{r}_R$ can be assured in advance. The choice of $\bar{r}_R$ might be influenced by the protection zones mentioned. However, if the aircraft turn rate has a limit $\bar{\Gamma}$, then Eq. (49) requires that $fV_R/4V^2 \le \bar{\Gamma}$, which is satisfied by choosing $f \le 4V^2\bar{\Gamma}/V_R$. This could be inconsistent with Eq. (64) if the aircraft were initially too

close and their courses were too convergent. Then the nominated safe separation could not be achieved. Other details of the motion can be obtained from the trigonometry of the circles.

If f is given by Eq. (6), then Eq. (63) becomes

$$\dot{M} = -\tfrac{1}{2}p\dot{r}_R \tag{65}$$

and so the rate of M is proportional to the closing speed. Then $M + \frac{1}{2}pr_R = c$ is a constant of the motion, determined by initial conditions. Thus, $r_R = 2c/p$ at EPG and UPE, and $\bar{r}_R = 2c/(p+2)$. Without further constraints, a specified $\bar{r}_R$ at the CPA is exceeded by choosing

$$p > 2\frac{\bar{r}_R - M(0)}{r_R(0) - \bar{r}_R} \tag{66}$$

The turning rates (34) reach a maximum of $pV_R/2\bar{r}_R$ at the CPA. Hence, the turning limit requires that $p(p+2) \le 4c\bar{\Gamma}/V_R$, which could be inconsistent with Eq. (66), as before. To describe the time dependence of the relative motion, we use Eqs. (10), (11), and (19) to get

$$\dot{r}_R = \pm\frac{V_R}{r_R}\sqrt{r_R^2 - M^2} = \pm\frac{V_R}{r_R}\sqrt{r_R^2 - (c - \frac{1}{2}pr_R)^2} \tag{67}$$

with the negative (positive) sign applying before (after) CPA. The integration can be performed explicitly to give t in terms of r_R. Likewise, one can get t in terms of M. The formulas can be used to obtain Fig. 3 directly. Some basic properties of the guidance follow from Eq. (67). First, it implies that $r_R(t)$ is symmetric in t about CPA, and then Eq. (65) implies that $M(t)$ is symmetric about CPA, which confirm Corollary 5.1. Second, Eq. (67) implies

$$\ddot{r}_R = \frac{1}{2}\frac{d\dot{r}_R^2}{dr_R} = \frac{V_R^2 c}{r_R^3}\left(c - \frac{1}{2}pr_R\right) > 0 \tag{68}$$

and so $r_R(t)$ is convex. Then Eq. (65) implies that $M(t)$ is concave. These properties are illustrated in Fig. 3. Also, $\ddot{r}_R = 0$ and $\ddot{M} = 0$ at EPG and UPE. Thus, both $r_R(t)$ and $M(t)$ evolve in ideal fashion.

Third, one can determine the general influence of p on r_R, which is now written as $r_R(t, p)$. Any initial state can be traced back to an EPG, which is taken, for simplicity, as the zero of time. Then $r_R(0, p) = 2c/p$, and integrating Eq. (67) yields

$$\int_{r_R(t,p)}^{r_R(0,p)} h(r, p)\mathrm{d}r = V_R t \tag{69}$$

before CPA, where

$$h(r, p) = \frac{r}{\sqrt{r^2 - \frac{1}{4}p^2[r_R(0, p) - r]^2}} \tag{70}$$

Noting that $h > 0$ and $\partial h/\partial p > 0$, it follows from Eq. (69) that $r_R(t, p) \uparrow$ as $p \uparrow$ for any fixed t. A similar conclusion is reached after CPA. Also, Eq. (66) implies that $\bar{r}_R \uparrow$ as $p \uparrow$. Thus, increasing p increases separation, which justifies the name of *gain constant* and shows that one has good control on separation through p.

If aircraft 2 is replaced by a fixed obstacle, then Eqs. (5) and (22) imply that

$$\dot{M} = -\frac{f_1 r_R \dot{r}_R}{V_1^2} \tag{71}$$

If f_1 is replaced by $f/2$, then this coincides with Eq. (63). Thus, the preceding formulas and properties all carry over after making this substitution. One can also obtain the path explicitly in polar coordinates, but the formula is rather complex and of little practical value.

Finally, if f has the more general product form $f = g(r_R)h(M)$, then a similar solution method can be used.

XII. Effectiveness of a Cockpit Display

A second major objective of this paper is prove that the cockpit display described in [31] has some basic desirable properties. This is achieved by proving that an ideal manual response to the display is equivalent to EMD guidance. Then the properties obtained for EMD guidance can also be attributed to the display in this idealized setting. Examples of this equivalence were used in [31].

For two conflicting aircraft, the display is obtained by calculating and displaying the EMD value M, not only for the actual 3-D heading of own aircraft, but for all hypothetical 3-D headings. One version of the display, designed as a head-up display, consists of contours of constant M projected stereographically. One such contour is sketched in Fig. 14. This shows the pilot how to steer away from directions with low M toward directions of high M. Thus, it provides the pilot with a direct indication of potential conflict associated with different steering directions, which is often difficult for pilots to estimate from current displays.

More precisely, one considers all hypothetical directions $\boldsymbol{u}_1$ of own aircraft's velocity vector $\boldsymbol{V}_1$, at the current actual speed V_1 and with the current $\boldsymbol{r}_1$, $\boldsymbol{r}_2$, and $\boldsymbol{V}_2$. The value $M(\boldsymbol{V}_1)$ of the EMD, on the unit sphere of possible $\boldsymbol{u}_1$ directions, is projected stereographically on the display and represented by contour lines of constant M (Fig. 14). The actual current $\boldsymbol{u}_1$ is located at the center of the display, indicated by the crosshairs.

Steering to increase EMD on the display is evidently similar to steering via EMD guidance. The general relationship is actually very close, as follows. As $\boldsymbol{V}_2$ is fixed for this calculation, Lemma 2 becomes

$$\frac{\partial M}{\partial \boldsymbol{V}_1} = \frac{r_R \dot{r}_R}{V_R^2}\boldsymbol{m} \tag{72}$$

Thus, $\boldsymbol{m}$ is normal to the level surfaces of $M(\boldsymbol{V}_1)$. Such a surface cuts the unit sphere on a contour, for which the normal at $\boldsymbol{u}_1$ on the sphere is $\bar{\boldsymbol{m}}_1$. According to Eqs. (4), the velocity of the point located at $\boldsymbol{u}_1$ on the sphere is

$$\dot{\boldsymbol{u}}_1 = -\frac{f_1}{V_1}\bar{\boldsymbol{m}}_1 \tag{73}$$

and so $\boldsymbol{u}_1$ moves normal to contours of constant M. When $\dot{r}_R < 0$ in Eq. (72), $\boldsymbol{u}_1$ moves in the direction of increasing M. The conclusion is summarized as follows.

Theorem 10. If two aircraft perform EMD guidance, then the crosshairs in an aircraft's display move normal to contours of constant M. When the aircraft are closing, the crosshairs move in the direction of increasing M.

This equivalence has implications about the performance of the display. If the idealized aircraft is steered manually by the pilot, and to move the crosshairs in the most effective way, normal to contours of constant M, then the aircraft performs a version of EMD guidance. Hence, the demonstrated properties of EMD guidance also apply when the aircraft are steered manually in this way. For example, Theorem 2 now shows that when manual steering leads to a local minimum of r_R, the aircraft are at the CPA, and so they never encounter the alarming prospect that r_R might subsequently decrease further. Also, Theorem 4 and Fig. 4 now indicate the turning

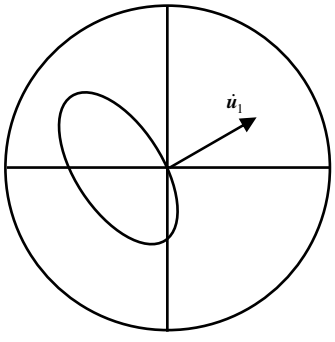

Fig. 14 The crosshairs move normal to a contour of constant M.

directions that result from manual steering according to the display, and these have a very logical basis. Thus, one can demonstrate some general outcomes of manual steering according to the display, which seems to be novel and desirable. The use of the display and its variants are described further in [31].

XIII. Conclusions

This paper is the first mathematical study of a particular guidance law for preventing a collision between two vehicles. The application studied is the midair collision of two aircraft, but the method has potential application to other types of guidable vehicles, such as spacecraft, ships, and submersibles, including robotic vehicles. The possible types of motion have been described in qualitative, geometric, and analytic terms. The results hold under general conditions and complement results for particular cases obtained by earlier simulations. Basic results about how the separation and expected miss distance change over time support the effectiveness of the guidance law. In some planar cases, simple formulas enable one to control, in advance, the separation at closest approach. The formulas show how this is influenced by limits on the turning capability of aircraft. In some cases, guidance generates paths that are arcs of circles: a very common and convenient aircraft maneuver.

The guidance law is completely consistent with a new cockpit display, so that ideal steering according to the display implies that a form of the guidance law is being followed. Hence, the established properties of the guidance also support the basic effectiveness of the display. This method of assessing a display seems to be novel and desirable and is possible because the display is based in a simple principle.

An aircraft has been modeled as a point mass with only 3 degrees of freedom. More realistic guidance and aircraft effects, including wind, could be considered. A more complete treatment of maneuvering limits is needed, including the different limits on vertical and horizontal maneuvers. Results obtained about the symmetry and congruence of paths might be extended to include force coefficients that are not isotropic, but only axially symmetric about a vertical axis. This would distinguish between horizontal and vertical maneuvers. Further evaluation of the method could be made by computer simulation of a large number of scenarios generated systematically or by Monte Carlo methods.

The method has been applied by other researchers to more than two vehicles by including priority rules and adding the pairwise command accelerations as though they contributed to a force field. The results presented here do not extend easily to such accelerations. For example, expected miss distances between pairs of vehicles do not always increase. The idea of adding command accelerations might be too simple, and the force field analogy might be overstretched. Then the challenge would be to formulate more suitable command accelerations. However, over the longer time scales on which multiple conflicts are managed, methods that generate planned paths might prove to be more suitable than real-time coordination.

Acknowledgments

The author thanks N. L. Fulton, R. Jarrett, T. Tarnopolskaya, M. Westcott, and the reviewers for their comments and suggestions.

References

[1] Swihart, D. E., Brannstrom, B., Griffin, E., Rosengren, R., and Doane, P., "A Sensor Integration Technique for Preventing Collisions Between Air Vehicles," *Proceedings of the 41st SICE Annual Conference*, Vol. 1, Inst. of Electrical and Electronics Engineers, Piscataway, NJ, Aug. 2002, pp. 625–629. doi:10.1109/SICE.2002.1195481

[2] Sporrong, J., and Uhlin, P., World Patent for a "System and Method for Avoidance of Collision Between Vehicles," Docket No. WO 01/46933 A1, filed 28 June 2001.

[3] Gazit, R. Y., and Powell, J. D., "Aircraft Collision Avoidance Based on GPS Position Broadcasts," *Proceedings of the 15th AIAA/IEEE Digital Avionics Systems Conference*, AIAA, Reston, VA, Oct. 1996, pp. 393–399.

[4] Khatib, O., "Real-Time Avoidance for Manipulators and Mobile Robots," *International Journal of Robotics Research*, Vol. 5, No. 1, Spring 1986, pp. 90–98. doi:10.1177/027836498600500106

[5] Krogh, B. H., "A Generalized Potential Field Approach to Obstacle Avoidance Control," *Proceedings of the SME Conference on Robotics Research: The Next Five Years and Beyond*, Bethlehem, PA, Aug. 1984.

[6] Tilove, R. B., "Local Obstacle Avoidance for Mobile Robots Based on the Method of Artificial Potentials," *Proceedings of the IEEE International Conference on Robotics and Automation*, Inst. of Electrical and Electronics Engineers, Piscataway, NJ, May 1990, pp. 566–571.

[7] Barraquand, J., Latombe, J.-C., "A Monte-Carlo Algorithm for Path Planning with Many Degrees of Freedom," *Proceedings of the IEEE International Conference on Robotics and Automation*, Inst. of Electrical and Electronics Engineers, Piscataway, NJ, May 1990, pp. 1712–1717.

[8] Kim, J. O., and Khosla, P. K., "Real-Time Obstacle Avoidance Using Harmonic Potential Functions," *IEEE Transactions on Robotics and Automation*, Vol. 8, 1992, pp. 338–349. doi:10.1109/70.143352

[9] Koditschek, D. E., "Exact Robotic Navigation by Means of Potential Functions: Some Topological Considerations," *Proceedings of the IEEE International Conference on Robotics and Automation*, Inst. of Electrical and Electronics Engineers, Piscataway, NJ, May 1987, pp. 1–6.

[10] Singh, L., Stephanou, H., and Wen, J., "Real-Time Robot Motion Control with Circulatory Fields," *Proceedings of the IEEE International Conference on Robotics and Automation*, Inst. of Electrical and Electronics Engineers, Piscataway, NJ, Apr. 1996, pp. 2737–2742.

[11] Masoud, A. A., and Bayoumi, M., "Robot Navigation Using the Vector Potential Approach," *Proceedings of the IEEE International Conference on Robotics and Automation*, Inst. of Electrical and Electronics Engineers, Piscataway, NJ, May 1993, pp. 805–811.

[12] Masoud, A. A., "Using Hybrid Vector Potential Fields for Multi-Robot, Multi-Target Navigation in a Stationary Environment," *Proceedings of the IEEE International Conference on Robotics and Automation*, Inst. of Electrical and Electronics Engineers, Piscataway, NJ, Apr. 1996, pp. 3564–3571.

[13] Keymeulen, D., and Decuyper, J., "Self-Organizing System for the Motion Planning of Mobile Robots," *Proceedings of the IEEE International Conference on Robotics and Automation*, Inst. of Electrical and Electronics Engineers, Piscataway, NJ, Apr. 1996, pp. 3369–3374.

[14] Zeghal, K., and Ferber, J., "A Reactive Approach for Distributed Air Traffic Control," *International Conference on Artificial Intelligence and Expert Systems*, Avignon, France, May 1993.

[15] Zeghal, K., "Airborne Conflict Detection and Resolution Using Coupled Force Fields: Principles and Results," *AGARD/NATO Workshop on Air Traffic Management*, Vol. 15, AGARD, Neuilly-sur-Seine, France, July 1997, pp. 1–11.

[16] de Medio, C., and Oriolo, G., "Robot Obstacle Avoidance Using Vortex Fields," *Advances in Robot Kinematics*, edited by S. Stifter, and A. Lenarcic, Springer–Verlag, New York, 1991, pp. 227–235.

[17] Kosecka, J., Tomlin, C., Pappas, G., and Sastry, S., "Generation of Conflict Resolution Maneuvers for Air Traffic Management," *Proceedings of the IEEE International Conference on Intelligent Robots and Systems*, Vol. 3, Inst. of Electrical and Electronics Engineers, Piscataway, NJ, Sept. 1997, pp. 1598–1603.

[18] Schaub, H., "Stabilization of Satellite Motion Relative to a Coulomb Spacecraft Formation," *Journal of Guidance, Control, and Dynamics*, Vol. 28, No. 6, Nov.–Dec. 2005, pp. 1231–1239. doi:10.2514/1.8577

[19] Beryman, J., and Schaub, H., "Analytical Charge Analysis for Two- and Three-Craft Coulomb Formations," *Journal of Guidance, Control, and Dynamics*, Vol. 30, No. 6, Nov.–Dec. 2007, pp. 1701–1710. doi:10.2514/1.23785

[20] Wang, S., and Schaub, H., "Spacecraft Collision Avoidance Using Coulomb Forces with Separation Distance Feedback," *Journal of Guidance, Control, and Dynamics*, Vol. 31, No. 3, May–June, 2008, pp. 740–750. doi:10.2514/1.29634

[21] Frazzoli, E., Mao, Z.–H., Oh, J.-H., and Feron, E., "Resolution of Conflicts Involving Many Aircraft Via Semi-Definite Programming," *Journal of Guidance, Control, and Dynamics*, Vol. 24, No. 1, Jan.–Feb. 2001, pp. 79–86. doi:10.2514/2.4678

[22] Tomlin, C., Mitchell, I., and Ghosh, R., "Safety Verification of Conflict Resolution Manoeuvres," *IEEE Transactions on Intelligent Transportation Systems*, Vol. 2, No. 2, June 2001, pp. 110–120. doi:10.1109/6979.928722

[23] Hu, J., Prandini, M., and Sastry, S., "Optimal Coordinated Maneuvers for Three-Dimensional Aircraft Conflict Resolution," *Journal of Guidance, Control, and Dynamics*, Vol. 25, No. 5, Sept.–Oct. 2002, pp. 888–900. doi:10.2514/2.4982

[24] Sultan, C., and Seereram, S., "Energy Suboptimal Collision-Free Reconfiguration for Spacecraft Formation Flying, *Journal of Guidance, Control, and Dynamics*, Vol. 29, No. 1, Jan.–Feb. 2006, pp. 190–192. doi:10.2514/1.10781

[25] Slater, G. L., Byram, S. M., and Williams, T. W., "Collision Avoidance for Satellites in Formation," *Journal of Guidance, Control, and Dynamics*, Vol. 29, No. 5, Sept.–Oct. 2006, pp. 1140–1146. doi:10.2514/1.16812

[26] Park, S., Deyst, J., and How, J. P., "Performance and Lyapunov Stability of a Nonlinear Path-Following Guidance Method," *Journal of Guidance, Control, and Dynamics*, Vol. 30, No. 6, Nov.–Dec. 2007, pp. 1718–1728. doi:10.2514/1.28957

[27] Kuchar, J. K., and Yang, L. C., "A Review of Conflict Detection and Resolution Modeling," *IEEE Transactions on Intelligent Transportation Systems*, Vol. 1, No. 4, Dec. 2000, pp. 179–189. doi:10.1109/6979.898217

[28] Frazzoli, E., Dahleh, M. A., and Feron, E., "Real-Time Motion Planning for Agile Autonomous Vehicles," *Journal of Guidance, Control, and Dynamics*, Vol. 25, No. 1, Jan.–Feb. 2002, pp. 116–129. doi:10.2514/2.4856

[29] Borst, C., Mulder, M., van Paasen, M. M., and Mulder, J. A., "Path-Oriented Control/Display Augmentation for Perspective Flight-Path Displays," *Journal of Guidance, Control, and Dynamics*, Vol. 29, No. 4, July–Aug. 2006, pp. 780–791. doi:10.2514/1.16469

[30] Zeghal, K., "A Comparison of Different Approaches Based on Force Fields for Coordination Among Multiple Mobiles," *Proceedings of the IEEE/RSJ International Conference on Intelligent Robots and Systems*, Inst. of Electrical and Electronics Engineers, Piscataway, NJ, Oct. 1998, pp. 273–278.

[31] Gates, D. J., Gates, E. A., Westcott, M., and Fulton, N. L., "Stereo Projections of Miss Distance in Some New Cockpit Display Formats," *Journal of Aircraft*, Vol. 45, No. 5, Sept.–Oct., 2008, pp. 1725–1735. doi:10.2514/1.35574

[32] Franklin, G. E., Powell, J. D., and Emami-Naeini, A., *Feedback Control of Dynamic Systems*, 4th ed., Prentice Hall, Upper Saddle River, NJ, 2002.

[33] Goldstein, H., *Classical Mechanics*, Addison-Wesley, Reading, MA, 1950, pp. 8, 58, 71, 194.

[34] Struik, D. J., *Lectures on Classical Differential Geometry*, 2nd ed., Dover, New York, 1988, pp. 13, 15, 29, 33.